Design, Fabrication, and Characterization of Scandium Aluminum Nitride-Based Piezoelectric Micromachined Ultrasonic Transducers

Qi Wang, *Student Member, IEEE*, Yipeng Lu, *Member, IEEE*, Sergey Mishin,
Yury Oshmyansky, and David A. Horsley, *Senior Member, IEEE*

***Abstract*— This paper presents the design, fabrication, and characterization of piezoelectric micromachined ultrasound transducers (PMUTs) based on scandium aluminum nitride ($Sc_xAl_{1-x}N$) thin films (x = 15%). ScAlN thin film was prepared with a dual magnetron system and patterned by a reactive ion etching system utilizing chlorine-based chemistry with an etching rate of 160 nm/min. The film was characterized by X-ray diffraction, which indicated a crystalline structure expansion compared with pure AlN and a well-aligned ScAlN film. ScAlN PMUTs were fabricated by a two-mask process based on cavity SOI wafers. ScAlN PMUTs with 50- and 40-μm diameter had a large dynamic displacement sensitivity measured in air of 25 nm/V at 17 MHz and 10 nm/V at 25 MHz, twice that of AlN PMUTs with the same dimensions. The peak displacement as a function of electrode coverage was characterized, with maximum displacement achieved with an electrode radius equal to 70% of the PMUT radius. Electrical impedance measurements indicated that the ScAlN PMUTs had 36% greater electromechanical coupling coefficient (k_t^2) compared with AlN PMUTs. The output pressure of a 7 × 7 ScAlN PMUT array was 0.7 kPa/V at ∼1.7 mm away from the array, which is approximately three times greater that of an 8 × 8 AlN PMUT array with the same element geometry and fill factor measured at the same distance. Acoustic spreading loss and PMUT insertion loss from mechanical transmit to receive were characterized with a 15 × 15 ScAlN PMUT array via hydrophone and laser Doppler vibrometer. [17509-2017]**

***Index Terms*— Piezoelectric micromachined ultrasound transducers (PMUT), piezoelectric films, piezoelectric transducers.**

I. INTRODUCTION

MANY applications have been developed based on micromachined ultrasonic transducers (MUTs) in recent years, such as medical imaging [1]–[3], gesture sensors [4], ultrasonic fingerprint sensors [5], and body-composition sensors [6]. MUTs have a better acoustic coupling, lower manufacturing cost and lower power consumption compared to conventional bulk ultrasonic transducers. Piezoelectric micromachined ultrasonic transducers (PMUT) have been rapidly developed in recent years due to the progress of piezoelectric thin films. Aluminum nitride (AlN) has been widely used for piezoelectric MEMS device fabrication because it is available from a number of MEMS foundries and is compatible with CMOS manufacturing [7]–[9]. However, compared to lead zirconate tianate (PZT), a piezoelectric material which requires high annealing temperature and is not process-compatible with CMOS, AlN has relatively low piezoelectric coefficient ($e_{31,f}$), which leads to low sensitivity and low electromechanical coupling (k_t^2) [9]–[11].

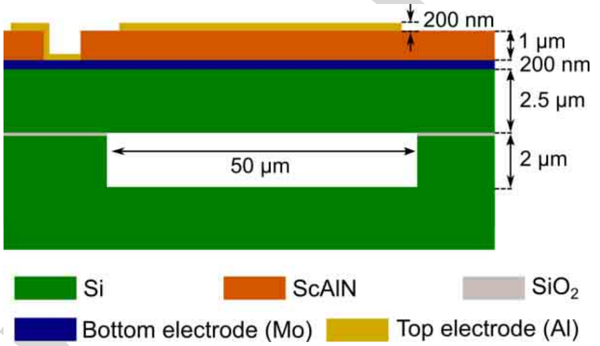

Fig. 1. Schematic cross-section of PMUT.

Scandium (Sc) alloying has been proposed recently as a means to increase the $e_{31,f}$ of AlN, while maintaining process compatibility with existing AlN based manufacturing [12]. Most of the previously-reported work on ScAlN focused on bulk acoustic wave (BAW) resonators or surface acoustic wave (SAW) devices which utilize the longitudinal piezoelectric mode and require high stiffness to achieve high frequency operation and high quality factor (Q) [12], [13]. However, studies also found that with the increase of Sc concentrations, the stiffness of the thin film decreased and the dielectric constant increased [14], [15]. In this paper, we present flexural PMUT devices which use the transverse piezoelectric mode and where the reduced stiffness of ScAlN may provide a benefit over conventional AlN.

II. MATERIALS AND METHODS

A cross-section schematic of a PMUT is shown in Fig. 1. The PMUT was composed of a 1 μm thick ScAlN

Manuscript received November 7, 2016; revised May 23, 2017; accepted May 26, 2017. This work was supported by Berkeley Sensor and Actuator industrial members. Subject Editor A. Seshia. *(Corresponding author: Qi Wang.)*

Q. Wang, Y. Lu, and D. A. Horsley are with the Department of Mechanical and Aerospace Engineering, University of California at Davis, Davis, CA 95616 USA (e-mail: qixwang@ucdavis.edu).

AQ:1 S. Mishin and Y. Oshmyansky are with Advanced Modular Systems, Inc., Goleta, CA, USA.

Color versions of one or more of the figures in this paper are available online at http://ieeexplore.ieee.org.

Digital Object Identifier 10.1109/JMEMS.2017.2712101

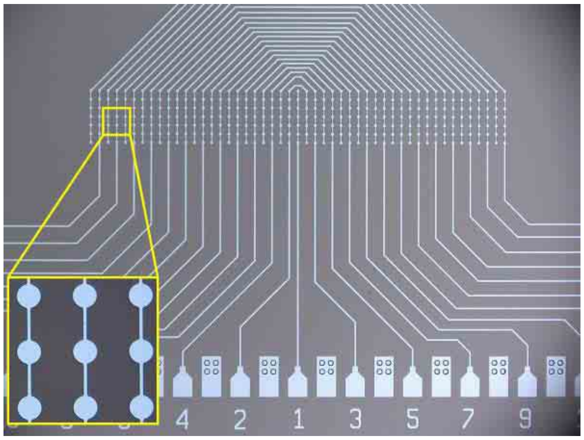

Fig. 2. An optical microscope image of a 7 × 49 PMUT array. The individual PMUTs are 50 μm diameter and the array pitch is 70 μm.

piezoelectric layer, a 200 nm Mo layer as bottom electrode and a 2.5 μm thick silicon membrane. Devices were also fabricated using pure AlN with identical film thicknesses and geometries in order to provide a comparison between ScAlN and AlN PMUTs. The fabrication process used custom cavity SOI (CSOI) substrates wherein vacuum cavities are formed beneath the Si device layer of the CSOI wafer [10]. This process avoids the need for through-wafer etching or sacrificial release layers and eliminates the possible squeeze-film damping between the PMUT membrane and the Si substrate. 150 mm diameter CSOI wafers (IceMOS Technologies) were manufactured with 2 μm deep cavities patterned with diameters from 40 μm to 50 μm and both individual PMUTs and 2D arrays of PMUTs were defined on the wafer. A 7 × 49 array composed of PMUTs with 50 μm diameter and 70 μm pitch is shown in Fig. 2.

The Mo and $Sc_xAl_{1-x}N$ (x = 15%) layers were sputtered in an Advanced Modular Systems (AMS) cluster tool with AlN deposition chambers and ion beam trimming module. The system used a standard dual conical magnetron with an AC deposition source operating at 40 kHz and power varying from 3 to 10 kW. The ScAlN deposition process was in deep poison mode using targets composed of Al and Sc pieces. High purity research grade argon and nitrogen process gases were used for the deposition. The base pressure of the process is ~5 mTorr and the process temperature is ~400 °C. Compared to Al-Sc alloy target and multiple targets of Al and Sc, multiple piece targets are easy to make and practical for high volume production. Locally adjusted magnetic field for target pieces of both Al and Sc guaranteed a constant thin film composition over the entire target life. Substrate rotation was utilized to compensate for the variation of the sputtering yield for different materials and composition non-uniformity across the substrate.

The CSOI wafers were cleaned by ion milling first in order to achieve a good interface for the following thin film deposition. A 30 nm thick ScAlN film was first deposited on the CSOI as a seed layer in order to achieve a good crystalline structure of the subsequent Mo and ScAlN layers. Then a 200 nm thick molybdenum (Mo) layer was sputtered as the bottom electrode in a different chamber in the system without breaking vacuum. Finally, 1 μm thick ScAlN was sputtered on the Mo layer. A cross-section scanning electron microscope (SEM) image of a PMUT, Fig. 3, shows the dense columnar structure of the ScAlN film and Mo bottom electrode.

Following deposition of the ScAlN layer, vias were opened to contact the Mo bottom electrode. AlN films are often etched using heated Microposit MF-319, a positive photoresist developer mainly composed of tetramethylammonium hydroxide (TMAH). However, experiments showed that the ScAlN etch rate in MF-319 was ~50 nm/min at 60 °C to 70 °C, approximately 4 times slower than that of AlN thin films at the same etching temperature. For this reason, reactive ion etching (RIE) in a transformer coupled plasma (TCP) etcher was studied using a combination of Cl_2 and BCl_3 gases with He used as diluent to improve etch uniformity. A 6.5 μm thick g-line photoresist (OCG 825 35S, Fujifilm) was spin coated, patterned, and hard baked for 16 hours to be used as a mask. An etch rate of 160 nm/min was achieved with the recipe shown in the Table I with an etching selectivity of 0.4 to the mask. Following the via etch, a 200 nm thick aluminum (Al) layer was evaporated and patterned by a lift-off process to form the top electrode and contact pads for the top and bottom electrodes.

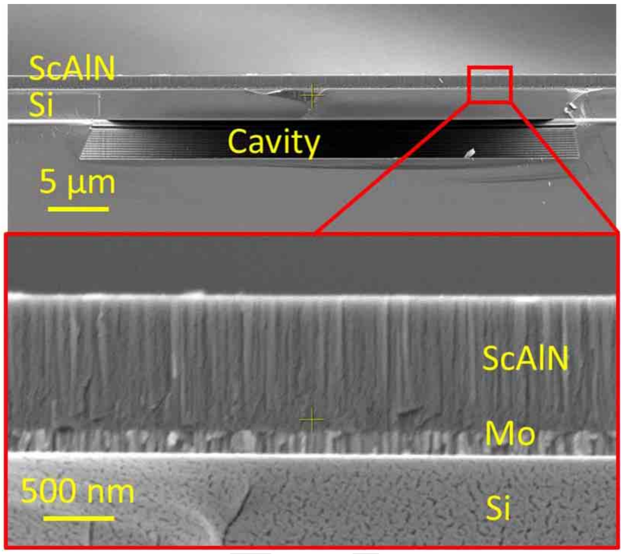

Fig. 3. Cross-sectional SEM image of a ScAlN PMUT. The Mo and ScAlN show good columnar structure indicating a highly c-axis oriented film.

TABLE I
RIE PARAMETERS

Parameter	Values
Cl_2 flow rate (sccm)	90
BCl_3 flow rate (sccm)	30
He flow rate (sccm)	100
TCP RF Power (W)	550
RF Bias Power (W)	150

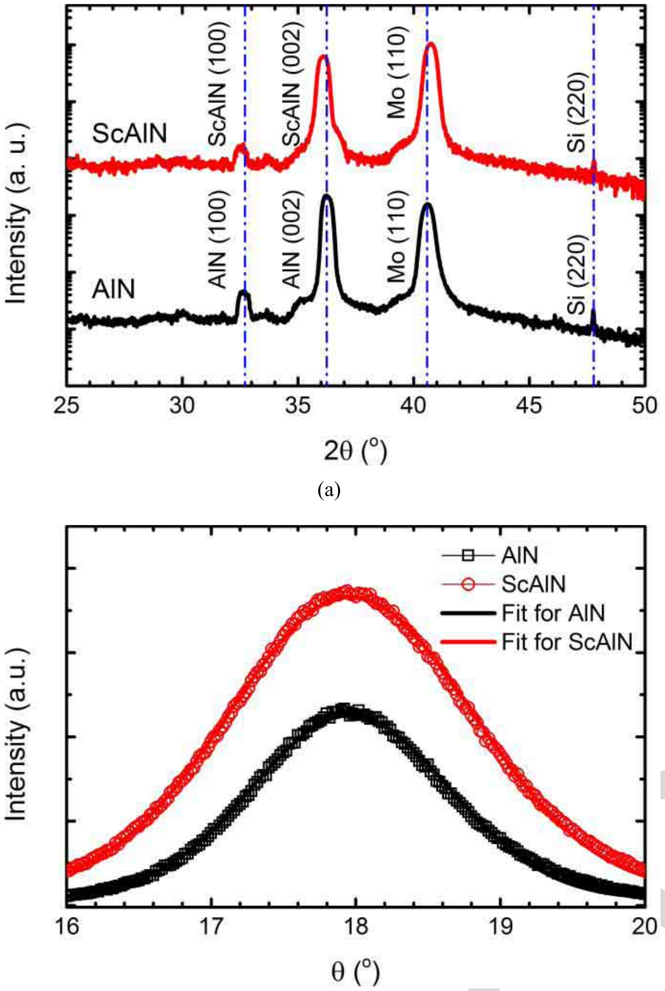

(a)

(b)

Fig. 4. (a) Normal coupled XRD measurement of ScAlN and AlN films in log scale; (b) Rocking curve measurement of the ScAlN and AlN (002) peak in linear scale.

III. Results

A. ScAlN film characterization

The ScAlN crystalline structure was studied using X-ray diffraction (XRD). Fig. 4(a) shows a comparison of the XRD peaks of pure AlN and ScAlN thin films on Mo electrode with 1 μm thickness. The (002) peak and small (100) peak of ScAlN were shifted to a slightly lower angle compared with that of AlN, indicating an expansion of the crystalline lattice according to Bragg's law. The rocking curve of the ScAlN (002) peak was also measured and is shown in Fig. 4(b). The full-width-half-maximum (FWHM) of the (002) peak is 1.6° for the AlN film and 1.9° for the ScAlN film, indicating that the c-axis of the ScAlN film is well aligned and predicting good piezoelectric properties [16].

A focused ion beam (FIB, Scios Dual Beam SEM/FIB system) was utilized to open a trench of approximate dimension 20 μm wide × 20 μm long × 10 μm deep on ScAlN thin film surface. The scandium concentration was measured on the cross section of ScAlN via energy dispersive X-ray spectroscopy (EDX, Oxford Instrument) at 15 keV beam energy. The EDX line-scan data is shown in Fig. 5. The results show a consistent scandium concentration of $x = 15$ at% throughout the thickness of the film. Note that the x-axis position of the EDX intensity in Fig. 5(a) is not exact due to the sample tilt in the SEM.

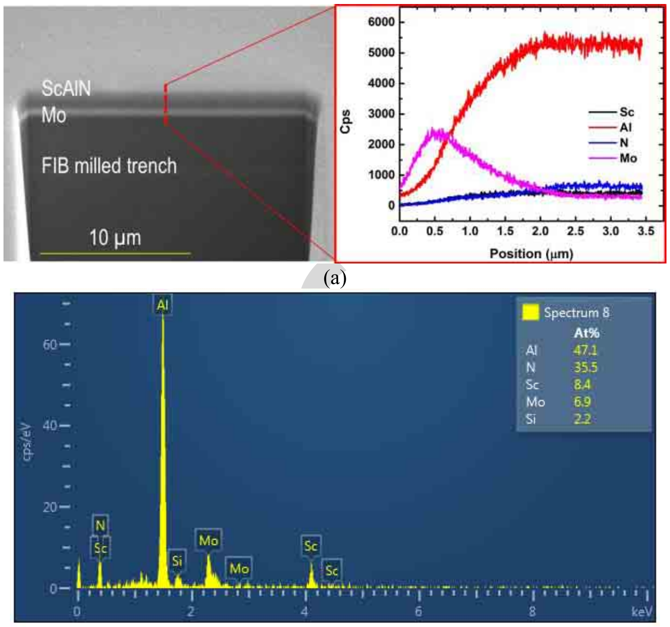

(a)

(b)

Fig. 5. (a) left: SEM image of FIB milled trench on ScAlN surface, right: EDX results over the line scan; (b) EDX results.

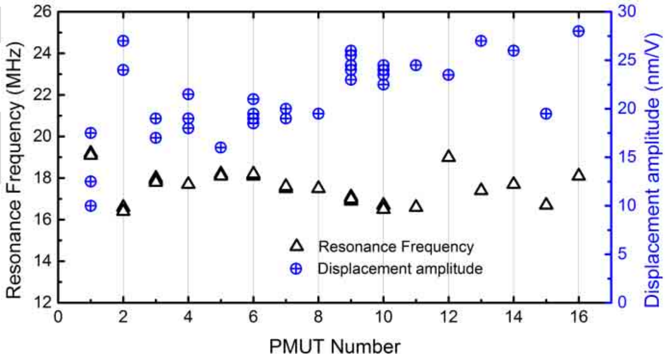

Fig. 6. Measured resonance frequency and dynamic displacement at resonance for ScAlN PMUT with 50 m diameter and 2.5 m nominal Si thickness.

B. Dynamic characterization

The frequency response of ScAlN PMUTs and AlN PMUTs with the same geometry were tested in air using a laser Doppler vibrometer (LDV, OFV 512 and OFV 2700, Polytec) in conjunction with a network analyzer (E5061B, Agilent Technology). LDV measurements were collected on 16 ScAlN PMUTs with 50 μm diameter selected from locations across one wafer, resulting in a 17.5 ± 1.5 MHz natural frequency, 22 ± 4 nm/V peak displacement sensitivity at resonance, and an average quality factor of $Q = 140$ in air. The die to die variation in resonant frequency was within 10% and the variation in amplitude was ∼20%. The results are shown in Fig. 6. Cross-section SEM images showed that

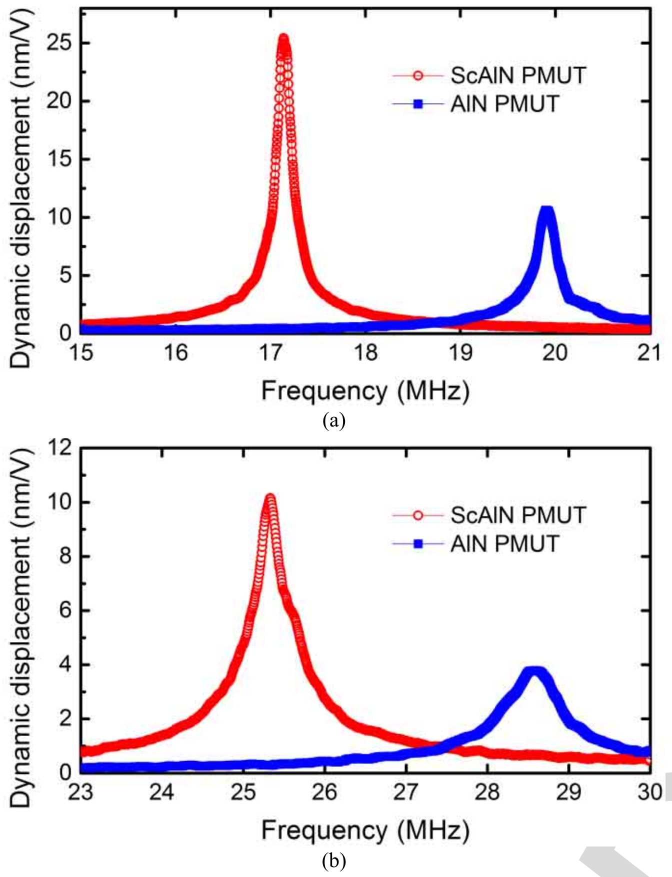

(a)

(b)

Fig. 7. LDV measurement results for (a) 50 μm diameter and (b) 40 μm diameter ScAlN and AlN PMUTs.

the Si thickness of these samples varied from 2.40 μm to 2.93 μm. Fig. 7 compares the LDV results of ScAlN and AlN PMUTs with 50 μm diameter and 40 μm diameter. The peak displacement of the ScAlN PMUTs are more than two times as large as that of the AlN devices.

The difference in the resonance frequency of ScAlN and AlN PMUTs is due to the stiffness reduction from Sc alloying. The resonant frequency of a circular PMUT can be computed from

$$f = \frac{1.63}{r^2}\sqrt{\frac{D}{\sum \rho_i t_i}} \tag{1}$$

where r is the PMUT radius, D is rigidity, ρ and t are the density and thickness of the Si, Mo, and ScAlN layers. The density of $Sc_{0.15}Al_{0.85}N$ is estimated to be 3430 kg/m^3, extrapolated from the density of $Sc_{0.4}Al_{0.6}N$ and AlN [15], [16]. The rigidity D can be expressed as

$$D = \frac{1}{3}\sum_{i=1}^{n}\frac{E_i^2(z_i^3 - z_{i-1}^3)}{1-\upsilon_i^2} \tag{2}$$

where E_i is the Young's modulus and ν_i is the Poisson's ratio of the material, z_i is the distance of the i-th layer top surface from the neutral axis. The Poisson's ratio of $Sc_{0.15}Al_{0.85}N$ in this paper is assumed to be 0.23 [15], [18]. Using (1), the Young's modulus of ScAlN was estimated to be 200 GPa ± 15 GPa, which is consistent with the reported values obtained from ScAlN BAW devices with similar Sc composition [19]. This formula also confirms that the measured variation in natural frequency across the wafer is consistent with the measured variation of the Si device layer thickness.

To extract an estimate of the transverse thin-film piezoelectric coefficient ($e_{31,f}$) from the frequency response data, we normalized the peak displacement by the quality factor, yielding an average value of $d_s = d_p/Q = 180$ pm/V. d_s is related to the transverse piezoelectric coefficient $e_{31,f}$ via [20]:

$$d_s = -r^2\frac{e_{31,f}(t_{si} + t_m + \frac{t_p}{2} - z_n)\cdot I_p(r)}{D\cdot I_d} \tag{3}$$

where t_{si} is the thickness of Si substrate, t_m is the thickness of bottom electrode, t_p is the thickness of ScAlN film, z_n is the distance from the middle of the ScAlN film to neutral axis, and $I_p(r)$ and I_d are integrals related to the piezoelectric bending moment and modal stiffness of the PMUT, both of which depend on the assumed vibration mode shape of the PMUT, $u(r)$,

$$I_p(r_e) = \int_0^{r_e}(r_e\frac{d^2u(r_e)}{dr_e^2} + \frac{du(r_e)}{dr_e})\cdot dr_e \tag{4}$$

$$I_d = \int_0^1[(\frac{d^2u(r)}{dr^2} + \frac{1}{r}\frac{du(r)}{dr})^2 - 2(1-\upsilon)\frac{1}{r}\frac{du(r)}{dr}\frac{d^2u(r)}{dr^2}]rdr \tag{5}$$

where υ is Poisson's ratio. $I_p(r_e)$ is a function of r_e, the radius of the circular top electrode normalized to the PMUT radius. Using $u(r) = (1-r^2)^2$ as the assumed mode shape for the 01 vibration mode of a circular membrane, (4) yields $I_p = -1$ at $r_e = 70\%$ and $I_d = 10.67$. Substituting these values along with the geometrical parameters into (3) yields an estimate of $e_{31,f} \sim 1.6$ C/m^2 which is ~60% higher than that of AlN. Our estimated value is consistent with the value extrapolated from [12] measured via a double-side beam interferometry (DBI) and slightly higher than the value extrapolated from [21] measured via a cantilever energy harvester.

Equation (3) also allows the optimum electrode radius for peak displacement to be identified. The estimated material properties including Young's modulus and $e_{31,f}$ were used in (3) to compute the theoretical displacement with r_e varying from 30% to 90%. The results are compared to experimental measurements of PMUTs with varying electrode diameters in Fig. 8, demonstrating good agreement between model and experiment, with the maximum displacement observed with electrode radius from 70% to 80% of the PMUT radius. The difference between theoretical and experimental results at 80% and 90% electrode coverage may be due to inexact boundary conditions (the model assumes perfect clamping at the membrane boundary while some flexing occurs in this location in the real device) or misalignment of the electrode to the silicon membrane (when the electrode covers nearly the whole membrane, an off-center electrode will be partly located on the anchor).

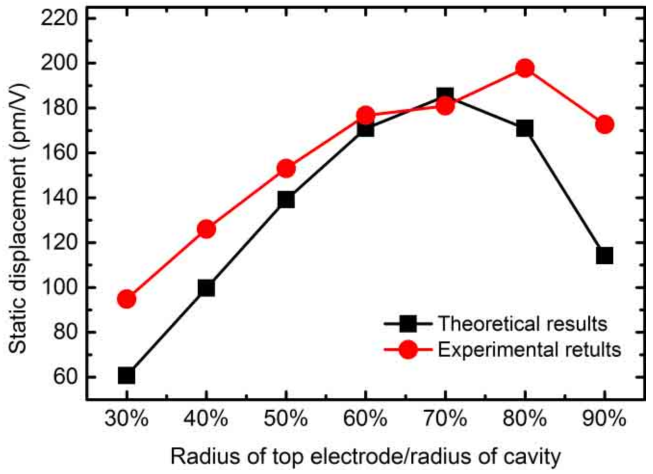

Fig. 8. Theoretical and experimental results of PMUT static displacement with different electrode radius.

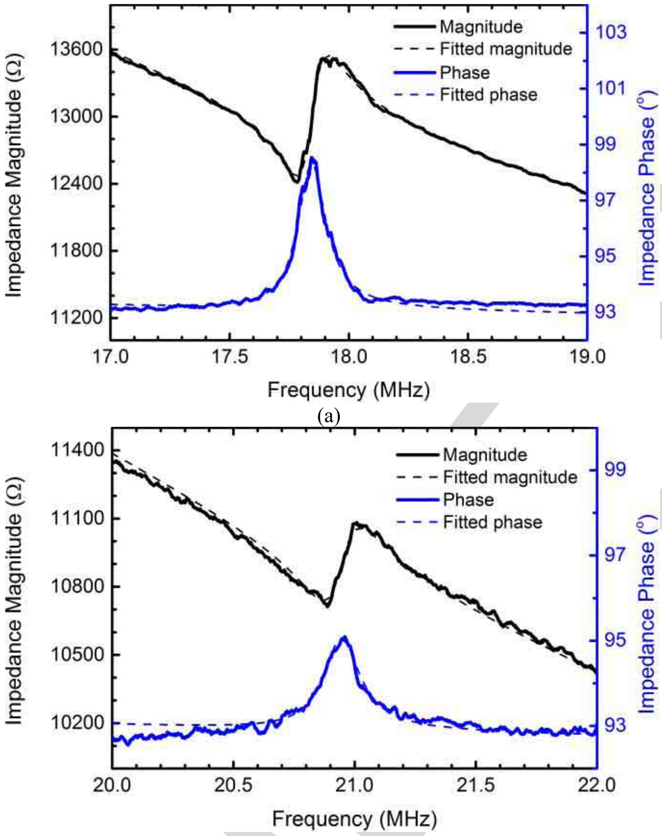

(a)

(b)

Fig. 9. Impedance measurement results for 50 μm diameter (a) ScAlN PMUT and (b) AlN PMUT.

C. Electrical characterization

Impedance measurements of ScAlN and AlN PMUTs, Fig. 9, were performed in air using a GSG RF probe calibrated with an impedance substrate standard (Cascade Microtech). The electromechanical coupling factor k_t^2 was calculated by:

$$k_t^2 = \frac{\pi^2}{4}\frac{f_r}{f_a}\frac{f_a - f_r}{f_a} \tag{6}$$

where f_a and f_r are the anti-resonant and resonant frequency respectively. The extracted k_t^2 was 1.9% for ScAlN PMUTs, consistent with the value calculated using the model presented in [20]. For AlN PMUTs, the extracted k_t^2 was 1.4%. This value is higher than the value calculated from the model (modeled AlN $k_t^2 = 0.8\%$). One source of error is that we subtracted the parasitic capacitance of the bond pads and probe setup, and the subtracted parasitic capacitance may have been larger than the true value. Comparing only the two extracted values, we find that the extracted k_t^2 of the ScAlN PMUT is 36% greater than that of AlN. The relative dielectric permittivity (ε_{ScAlN}) of ScAlN was also estimated from the impedance test as ∼12 which is around 20% higher than that of pure AlN. The estimated dielectric permittivity is consistent with the value reported in [12].

TABLE II
COMPARISON OF PIEZOELECTRIC MATERIAL PROPERTIES

Materials	$e_{31,f}$ (C/m^2)	ε_{33}	E (GPa)	$\frac{e_{31,f}^2}{\varepsilon_0\varepsilon_{33}}$ (GPa)
PZT [17]	-14.0	1200	65	18.5
AlN (this work)	-1.05	10.5	330	10.8
ScAlN (this work)	-1.6	12	200	24.1

We also calculated the electromechanical coupling factor using an alternative method to the impedance method described above. The 31 electromechanical coupling coefficient is defined as $k_{31}^2 \propto e_{31,f}^2/\varepsilon_{33}$ [22], [23]. For pulse-echo performance, this metric can be interpreted as follows – the square of the piezocoefficient appears in the numerator because both the TX and RX operations require energy conversion between the electrical and mechanical domains, while the dielectric constant is in the denominator because the RX charge is converted to a voltage by dividing by the capacitance. AlN, ScAlN, and PZT are compared in Table II using the extracted material parameters reported here. Note that while PZT is superior to AlN, the figure-of-merit for ScAlN is 30% greater than that of PZT. One caveat to this conclusion is that the presence of parasitic capacitance (e.g. due to bond-pads or cables between the PMUT and the receive amplifier) will greatly degrade the RX signal amplitude of a ScAlN or AlN PMUT due to the much lower dielectric constant of these materials. For example, a 50 μm diameter PMUT with $r_e = 70\%$ and a 1 μm thick ScAlN layer has a capacitance of 0.1 pF, so the presence of a 1 pF bond-pad capacitance will reduce the RX voltage by a factor of 11 (=0.1 pF /1.1 pF). In comparison, a PZT PMUT of the same size has 100 times greater capacitance, so a 1 pF parasitic capacitance would have negligible effect on the RX voltage.

D. Acoustic characterization

An array of ScAlN PMUTs was immersed in non-conductive fluid (Fluorinert FC-70, 3M) and the output acoustic pressure was measured with a 70 μm diameter needle hydrophone (Precision Acoustic, Inc.). The results are shown

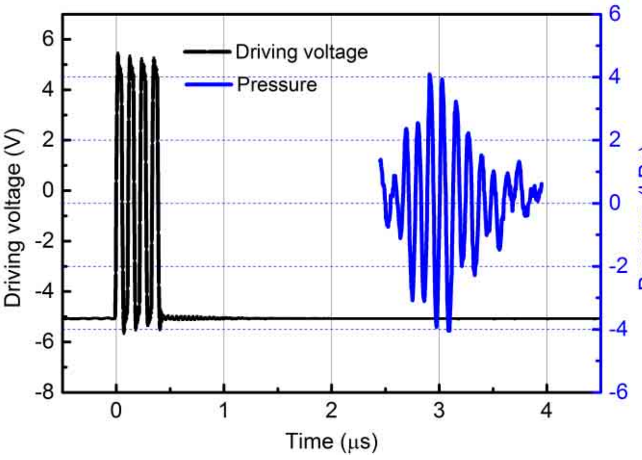

Fig. 10. Pressure measurement results for 7 × 7 ScAlN PMUT array.

TABLE III
COMPARISON OF ACOUSTIC TRANSMISSION PERFORMANCE

Material	Operation Frequency (MHz)	Drive Voltage (V)	Pressure (kPa)	Array size	Normalized output pressure (kPa/V/mm^2)
PZT [10]	10	25	58	9x9	2.52
AlN (this work)	9	25	6	8x8	0.34
ScAlN (this work)	9	11	8	7x7	1.40

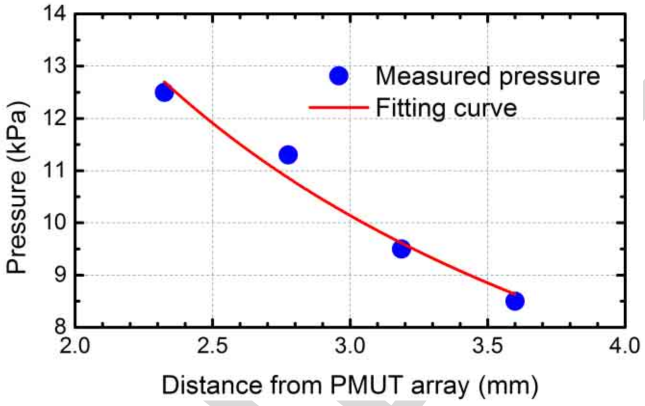

Fig. 11. Acoustic pressure measured from a 15 × 15 PMUT array.

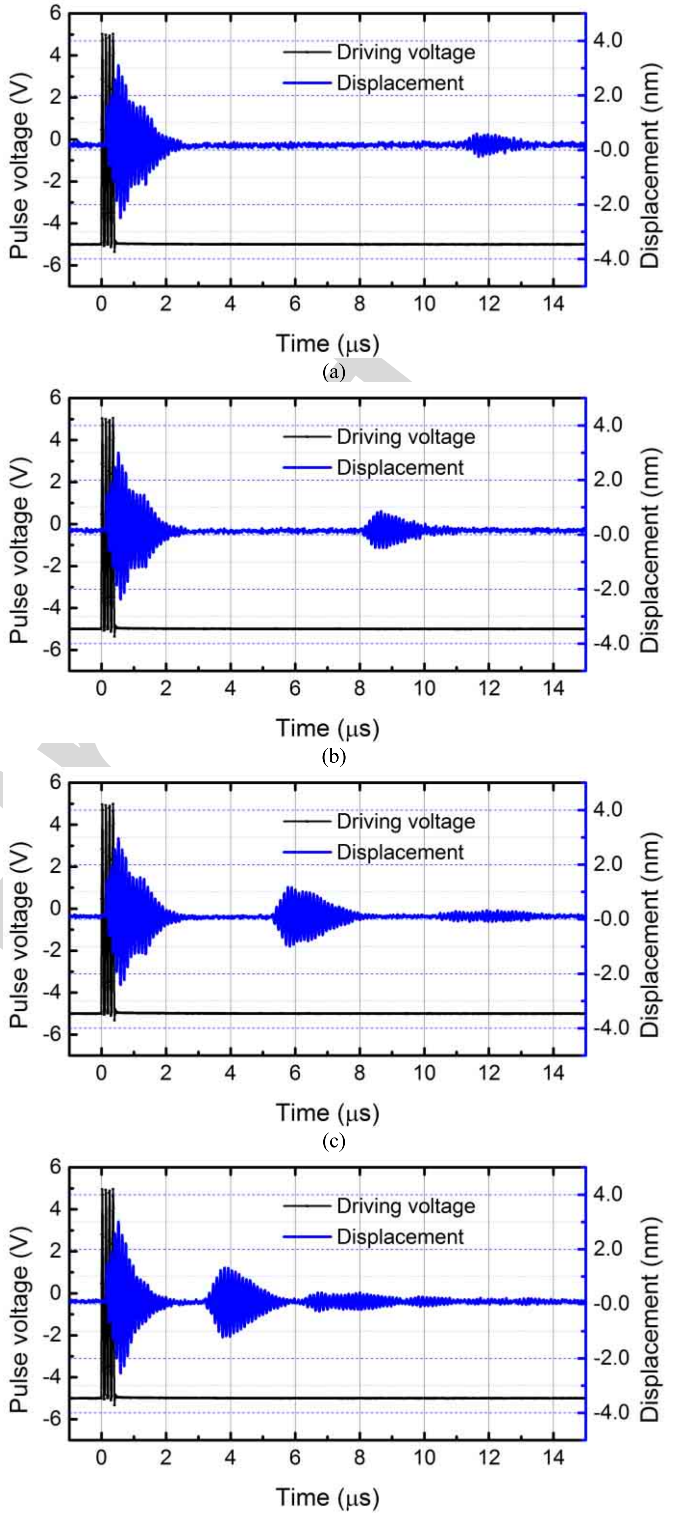

(a)

(b)

(c)

(d)

Fig. 12. LDV measurement of pulse-echo from a ScAlN PMUT in the center of 15 × 15 array with different Fluorinert heights of 4 mm, 3 mm, 2 mm and 1.2 mm.

AQ:2

in Fig. 10. A 7 × 7 ScAlN PMUT array was driven by four 9 MHz 11 Vpp pulses from a function generator (Rigol, DG-4102). The measured pressure generated by the ScAlN PMUT array was detected at ~2.5 μs after the pulse generation, which corresponds to ~1.7 mm from the PMUT surface to the hydrophone. The peak-to-peak pressure detected was ~8 kPa, which was 30% larger than ~6 kPa pressure generated from a 8 × 8 AlN PMUT array driven at 25 Vpp, suggesting 3x greater transmit efficiency from the ScAlN array. The acoustic transmitting performance of ScAlN, AlN and PZT PMUT arrays were compared as shown in Table III. The normalized output pressure represents the acoustic pressure output from a 1 mm^2 PMUT array area at a distance ~1.5 mm away from PMUT surface under 1 V driving voltage. The normalized pressure output of the ScAlN PMUT array presented

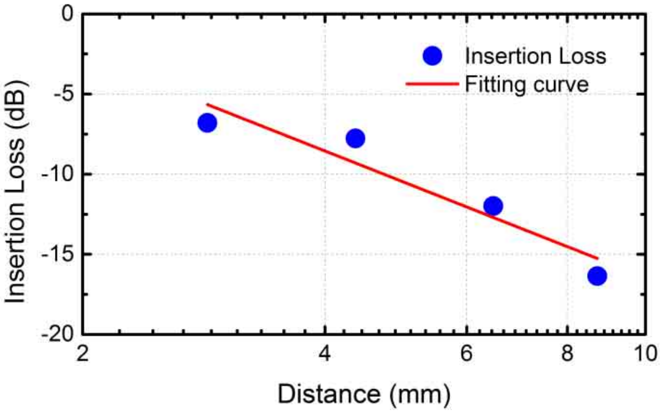

Fig. 13. Measured insertion loss from TX to RX vibration amplitudes as a function of round-trip pulse-echo distance.

here is ~55% of the PZT array presented in [10]. Considering the much smaller capacitance of ScAlN, we expect that the pulse-echo performance of the PZT and ScAlN arrays should be comparable, because the ScAlN array should have higher receive sensitivity.

The output acoustic pressure of a 15 × 15 ScAlN PMUT array was measured via hydrophone at different distances to PMUT surface. The measured peak-to-peak pressure versus distance is shown in Fig. 11. The result shows that the pressure decays inversely with the radial distance from the array [24]:

$$P\,(r) = P_0 R_0 x^{-1} \tag{7}$$

where R_0 is the Rayleigh distance and P_0 is the theoretical surface pressure. A fit of (7) to the experimental data gives $R_0 = 2.9$ mm and $P_0 = 20.6$ kPa. Given that the peak-to-peak displacement is 5 nm, the value of P_0 gives a transmit sensitivity of $S_{\mathrm{TX}} = 4$ kPa/nm.

The dynamic displacement of a 15 × 15 ScAlN PMUT array driven with 11 Vpp and immersed in fluid was measured via LDV, Fig. 12. An ~5 nm displacement of the center ScAlN PMUT was measured during the transmit (TX) excitation. PMUT vibration due to received (RX) echoes returning from the fluid-air surface were also visible in these experiments. The Fluorinert-air surface was varied from 4 mm to 1.2 mm, and the plots in Fig. 12 show the echoes return 11 μs, 8 μs, 5 μs and 3 μs after the TX pulse is sent. The corresponding round-trip distances calculated from these pulse echo measurements are consistent with the Fluorinert height using $c = 750$ m/s as the speed of sound in Fluorinert. In Fig. 12(c) and (d), a second echo can be observed due to the short liquid distance and large output pressure. The vibration amplitude of the first received echo relative to the transmit vibration amplitude fits the acoustic spreading model from (7),

$$d_{RX}(x)/d_{TX} = R_0 x^{-1} \tag{8}$$

This model is plotted along with the experimental data in dB units in Fig. 13. Comparing the experimental pressure measurements from Fig. 11 with the RX vibration amplitudes shown in Fig. 12, the receive sensitivity of the array is estimated to be $S_{\mathrm{RX}} = 0.25$ nm/kPa. Since the PMUT is a reciprocal transducer, $S_{\mathrm{TX}} = S_{\mathrm{RX}}^{-1}$, as expected.

IV. CONCLUSION

The results presented here demonstrate that ScAlN PMUTs have better performance than PMUTs made with AlN. Using 15% Sc, the transmit amplitude was increased by a factor of two relative to PMUTs made with pure AlN, consistent with a 60% increase in the transverse piezoelectric coefficient, $e_{31,f}$. The PMUT fabrication process is nearly unchanged by introducing ScAlN. While wet etching of $\mathrm{Sc_{0.15}Al_{0.85}N}$ in TMAH proceeds at a much slower etch rate than pure AlN, a $\mathrm{Cl_2/BCl_3}$plasma etch was demonstrated to achieve an etch rate of 120 nm/min for $\mathrm{Sc_{0.15}Al_{0.85}N}$. We expect that increasing the Sc concentration would further improve PMUT performance, since other work has shown that the piezoelectric coefficients of ScAlN increase as the Sc concentration is increased up to 40%. While RF devices, such as BAW filters, may suffer due to the reduced stiffness (and therefore lower acoustic velocity) that occurs as the Sc concentration is increased, this reduced stiffness does not degrade the performance of PMUTs.

ACKNOWLEDGMENT

The authors thank UC Berkeley Marvel Nanolab for the advice and help on the fabrication process, and IceMOS Technology for providing cavity SOI wafers.

REFERENCES

[1] Q. Wang *et al.*, “Scandium doped aluminum nitride based piezoelectric micromachined ultrasound transducers,” in *Proc. Solid-State Sens., Actuators, Microsyst. Workshop*, Hilton Head, SC, USA, 2016, pp. 436–439.

[2] D. E. Dausch, K. H. Gilchrist, J. B. Carlson, S. D. Hall, J. B. Castellucci, and O. T. V. Ramm, “*In vivo* real-time 3-D intracardiac echo using PMUT arrays,” *IEEE Trans. Ultrason., Ferroelectr., Freq. Control*, vol. 61, no. 10, pp. 1754–1764, Oct. 2014.

[3] Y. Lu *et al.*, “Waveguide piezoelectric micromachined ultrasonic transducer array for short-range pulse-echo imaging,” *Appl. Phys. Lett.*, vol. 106, no. 19, p. 193506, May 2015.

[4] R. J. Przybyla, H. Y. Tang, S. E. Shelton, D. A. Horsley, and B. E. Boser, “3D ultrasonic gesture recognition,” in *IEEE Int. Solid-State Circuits Conf. (ISSCC) Dig. Tech. Papers*, Feb. 2014, pp. 210–211.

[5] Y. Lu *et al.*, “Ultrasonic fingerprint sensor using a piezoelectric micromachined ultrasonic transducer array integrated with complementary metal oxide semiconductor electronics,” *Appl. Phys. Lett.*, vol. 106, no. 26, p. 263503, 2015.

[6] H.-Y. Tang, Y. Lu, S. Fung, D. A. Horsley, and B. E. Boser, “Integrated ultrasonic system for measuring body-fat composition,” in *IEEE Int. Solid-State Circuits Conf. (ISSCC) Dig. Tech. Papers.*, Feb. 2015, pp. 1–3.

[7] D. A. Horsley *et al.*, “Piezoelectric micromachined ultrasonic transducers in consumer electronics: The next little thing?” in *Proc. IEEE 29th Int. Conf. Micro Electro Mech. Syst. (MEMS)*, Jan. 2016, pp. 145–148.

[8] R. Ruby and P. Merchant, “Micromachined thin film bulk acoustic resonators,” in *Proc. 48th. IEEE Int. Freq. Control Symp.*, Jun. 1994, pp. 135–138.

[9] J. Zou, C.-M. Lin, Y.-Y. Chen, and A. P. Pisano, “Theoretical study of thermally stable $\mathrm{SiO_2/AlN/SiO_2}$ Lamb wave resonators at high temperatures,” *J. Appl. Phys.*, vol. 115, no. 9, p. 094510, Mar. 2014.

[10] Y. Lu and D. A. Horsley, “Modeling, fabrication, and characterization of piezoelectric micromachined ultrasonic transducer arrays based on cavity SOI wafers,” *J. Microelectromech. Syst.*, vol. 24, no. 4, pp. 1142–1149, 2015.

[11] Q. Wang, H. Oguchi, M. Hara, and H. Kuwano, “Investigation of dominant factors to control c-axis tilt angle of aln thin films for efficient energy harvesting,” in *Proc. IEEE 27th Int. Conf. Micro Electro Mech. Syst. (MEMS)*, Jan. 2014, pp. 636–639.

[12] R. Matloub *et al.*, "Piezoelectric $Al_{1-x}Sc_xN$ thin films: A semiconductor compatible solution for mechanical energy harvesting and sensors," *Appl. Phys. Lett.*, vol. 102, no. 15, p. 152903, Apr. 2013.

[13] M. Moreira, J. Bjurström, I. Katardjev, and V. Yantchev, "Aluminum scandium nitride thin-film bulk acoustic resonators for wide band applications," *Vacuum*, vol. 86, no. 1, pp. 23–26, Jul. 2011.

[14] K. Hashimoto, S. Sato, A. Teshigahara, T. Nakamura, and K. Kano, "High-performance surface acoustic wave resonators in the 1 to 3 GHz range using a ScAlN/6H-SiC structure," *IEEE Trans. Ultrason., Ferroelectr., Freq. Control*, vol. 60, no. 3, pp. 637–642, Mar. 2013, doi: 10.1109/TUFFC.2013.2606

[15] A. Konno *et al.*, "Determination of full material constants of ScAlN thin film from bulk and leaky Lamb waves in MEMS-based samples," in *Proc. IEEE Int. Ultrason. Symp.*, Sep. 2014, pp. 273–276.

[16] H. P. Loebl, M. Klee, C. Metzmacher, W. Brand, R. Milsom, and P. Lok, "Piezoelectric thin AlN films for bulk acoustic wave (BAW) resonators," *Mater. Chem. Phys.*, vol. 79, nos. 2–3, pp. 143–146, Apr. 2003.

[17] J.-M. Wagner and F. Bechstedt, "Properties of strained wurtzite GaN and AlN: Ab initio studies," *Phys. Rev. B, Condens. Matter*, vol. 66, no. 11, p. 115202, Sep. 2002.

[18] A. V. Sotnikov, H. Schmidt, M. Weihnacht, E. P. Smirnova, T. Y. Chemekova, and Y. N. Makarov, "Elastic and piezoelectric properties of AlN and $LiAlO_2$ single crystals," *IEEE Trans. Ultrason. Ferroelectr. Freq. Control*, vol. 57, no. 4, pp. 808–811, Apr. 2010.

[19] K. Umeda, H. Kawai, A. Honda, M. Akiyama, T. Kato, and T. Fukura, "Piezoelectric properties of ScAlN thin films for piezo-MEMS devices," in *Proc. IEEE 26th Int. Conf. Micro Electro Mech. Syst. (MEMS)*, Jan. 2013, pp. 733–736.

[20] M. Dubois and P. Muralt, "PZT thin film actuated elastic fin micromotor," *IEEE Trans. Ultrason., Ferroelectr., Freq. Control*, vol. 45, no. 5, pp. 1169–1177, Sep. 1998.

[21] P. M. Mayrhofer *et al.*, "ScAlN MEMS cantilevers for vibrational energy harvesting purposes," *J. Microelectromech. Syst.*, vol. 26, no. 1, pp. 102–112, 2016.

[22] P. Muralt and J. Baborowski, "Micromachined ultrasonic transducers and acoustic sensors based on piezoelectric thin films," *J. Electroceram.*, vol. 12, nos. 1–2, pp. 101–108, 2004.

[23] K. Smyth and S.-G. Kim, "Experiment and simulation validated analytical equivalent circuit model for piezoelectric micromachined ultrasonic transducers," *IEEE Trans. Ultrason. Ferroelectr. Freq. Control*, vol. 62, no. 4, pp. 744–765, Apr. 2015.

[24] D. T. Blackstock, *Fundamentals of Physical Acoustics*. Hoboken, NJ, USA: Wiley, 2000.

Qi Wang (S'15) received the B.S. degree in mechanical engineering and automation from the Nanjing University of Aeronautics and Astronautics, Nanjing, China, in 2011, and the M.S. degree in nanomechanics from Tohoku University, Sendai, Japan, in 2013.

He is currently pursuing the Ph.D. degree in mechanical engineering with the Department of Mechanical and Aerospace Engineering, University of California at Davis (UCD), Davis. He is also a Graduate Student Researcher with the Berkeley Sensor and Actuator Center, UCD. His research interests include piezoelectric thin films and MEMS sensors and actuators.

Yipeng Lu received the B.S. degree in materials science and engineering from Jilin University, Changchun, China, in 2007; the M.S. degree in microelectronics from Shanghai Jiao Tong University, Shanghai, China, in 201~~0,~~ and the Ph.D. degree in mechanical engineering from the University of California at Davis (UCD), Davis, CA, USA, in 2015. He joined the Berkeley Sensor and Actuator Center, UCD, as a Graduate Student Researcher. He was a Digital Hardware Engineer at Huawei in 2011. He is currently a Senior Engineer with Qualcomm. His research interests include MEMS sensors and actuators.

Sergey Mishin received the M.Phys. degree (Hons.) from the Russian National Research University of Electronic Technology in 1986.

His main research interests include cold discharge, high density plasma, magnetron plasma, excimer laser systems, and the application of plasma discharge and lasers in the semi-conductor industry.

He founded Advanced Modular Systems, Inc. in 2000. Advanced Modular Systems, Inc. is responsible for developing the first production worthy cluster tool for high volume piezoelectric thin films. By its second year, Advanced Modular Systems, Inc. was presented with the Supplier of the Year Award by Agilent Technologies, Inc. Since founding his company, he has been focused on the development of new equipment for the manufacture and treatment of piezoelectric thin films. As part of this research and development, he has had an opportunity to work closely with industry leaders and high-class research laboratories. He has also authored or co-authored numerous papers, and holds patents on the deposition and trimming technologies used in FBAR/BAW/SAW and MEMS application.

Yury Oshmyansky received the B.S. and M.S. degrees from the Colorado School of Mines. He was at Hewlett-Packard and subsequently Vitesse, Motorola, SFI, Agilent, Avago, and Advanced Modular Systems, Inc. He is currently the Director of process development with Advanced Modular Systems, Inc. He is also a Chemical Engineer. He holds many patents, and has published numerous papers in the field of manufacturing of the FBAR filters and related technologies.

AQ:3

David A. Horsley (M'97) received the B.S., M.S., and Ph.D. degrees in mechanical engineering from the University of California at Berkeley, Berkeley, CA, in 1992, 1994, and 1998, respectively. He has been a Co-Director of the Berkeley Sensor and Actuator Center since 2005. He held research and development positions at Dicon Fiberoptics, Hewlett Packard Laboratories, and Onix Microsystems. He is currently a Professor with the Department of Mechanical and Aerospace Engineering, University of California at Davis, Davis, CA. His research interests include microfabricated sensors and actuators with applications in ultrasonics and physical sensors. He was a recipient of the NSF CAREER Award and the UC Davis College of Engineering's Outstanding Junior Faculty Award.

AUTHOR QUERIES

AUTHOR PLEASE ANSWER ALL QUERIES

PLEASE NOTE: We cannot accept new source files as corrections for your paper. If possible, please annotate the PDF proof we have sent you with your corrections and upload it via the Author Gateway. Alternatively, you may send us your corrections in list format. You may also upload revised graphics via the Author Gateway.

AQ:1 = Please provide the postal code for “Advanced Modular Systems, Inc.”
AQ:2 = Please provide descriptions of all labeled subparts for Fig. 12.
AQ:3 = The term “AMSystems” has been changed to “Advanced Modular Systems, Inc.” Please confirm.

Design, Fabrication, and Characterization of Scandium Aluminum Nitride-Based Piezoelectric Micromachined Ultrasonic Transducers

Qi Wang, *Student Member, IEEE*, Yipeng Lu, *Member, IEEE*, Sergey Mishin,
Yury Oshmyansky, and David A. Horsley, *Senior Member, IEEE*

***Abstract*— This paper presents the design, fabrication, and characterization of piezoelectric micromachined ultrasound transducers (PMUTs) based on scandium aluminum nitride ($Sc_xAl_{1-x}N$) thin films (x = 15%). ScAlN thin film was prepared with a dual magnetron system and patterned by a reactive ion etching system utilizing chlorine-based chemistry with an etching rate of 160 nm/min. The film was characterized by X-ray diffraction, which indicated a crystalline structure expansion compared with pure AlN and a well-aligned ScAlN film. ScAlN PMUTs were fabricated by a two-mask process based on cavity SOI wafers. ScAlN PMUTs with 50- and 40-μm diameter had a large dynamic displacement sensitivity measured in air of 25 nm/V at 17 MHz and 10 nm/V at 25 MHz, twice that of AlN PMUTs with the same dimensions. The peak displacement as a function of electrode coverage was characterized, with maximum displacement achieved with an electrode radius equal to 70% of the PMUT radius. Electrical impedance measurements indicated that the ScAlN PMUTs had 36% greater electromechanical coupling coefficient (k_t^2) compared with AlN PMUTs. The output pressure of a 7 × 7 ScAlN PMUT array was 0.7 kPa/V at ∼1.7 mm away from the array, which is approximately three times greater that of an 8 × 8 AlN PMUT array with the same element geometry and fill factor measured at the same distance. Acoustic spreading loss and PMUT insertion loss from mechanical transmit to receive were characterized with a 15 × 15 ScAlN PMUT array via hydrophone and laser Doppler vibrometer. [17509-2017]**

***Index Terms*— Piezoelectric micromachined ultrasound transducers (PMUT), piezoelectric films, piezoelectric transducers.**

I. INTRODUCTION

MANY applications have been developed based on micromachined ultrasonic transducers (MUTs) in recent years, such as medical imaging [1]–[3], gesture sensors [4], ultrasonic fingerprint sensors [5], and body-composition sensors [6]. MUTs have a better acoustic coupling, lower manufacturing cost and lower power consumption compared to conventional bulk ultrasonic transducers. Piezoelectric micromachined ultrasonic transducers (PMUT) have been rapidly developed in recent years due to the progress of piezoelectric thin films. Aluminum nitride (AlN) has been widely used for piezoelectric MEMS device fabrication because it is available from a number of MEMS foundries and is compatible with CMOS manufacturing [7]–[9]. However, compared to lead zirconate tianate (PZT), a piezoelectric material which requires high annealing temperature and is not process-compatible with CMOS, AlN has relatively low piezoelectric coefficient ($e_{31,f}$), which leads to low sensitivity and low electromechanical coupling (k_t^2) [9]–[11].

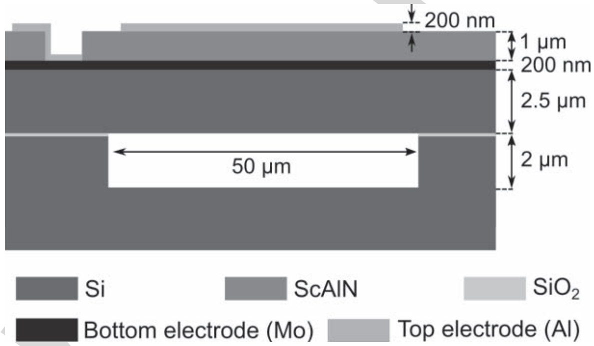

Fig. 1. Schematic cross-section of PMUT.

Scandium (Sc) alloying has been proposed recently as a means to increase the $e_{31,f}$ of AlN, while maintaining process compatibility with existing AlN based manufacturing [12]. Most of the previously-reported work on ScAlN focused on bulk acoustic wave (BAW) resonators or surface acoustic wave (SAW) devices which utilize the longitudinal piezoelectric mode and require high stiffness to achieve high frequency operation and high quality factor (Q) [12], [13]. However, studies also found that with the increase of Sc concentrations, the stiffness of the thin film decreased and the dielectric constant increased [14], [15]. In this paper, we present flexural PMUT devices which use the transverse piezoelectric mode and where the reduced stiffness of ScAlN may provide a benefit over conventional AlN.

II. MATERIALS AND METHODS

A cross-section schematic of a PMUT is shown in Fig. 1. The PMUT was composed of a 1 μm thick ScAlN

Manuscript received November 7, 2016; revised May 23, 2017; accepted May 26, 2017. This work was supported by Berkeley Sensor and Actuator industrial members. Subject Editor A. Seshia. *(Corresponding author: Qi Wang.)*

Q. Wang, Y. Lu, and D. A. Horsley are with the Department of Mechanical and Aerospace Engineering, University of California at Davis, Davis, CA 95616 USA (e-mail: qixwang@ucdavis.edu).

S. Mishin and Y. Oshmyansky are with Advanced Modular Systems, Inc., Goleta, CA, USA.

Color versions of one or more of the figures in this paper are available online at http://ieeexplore.ieee.org.

Digital Object Identifier 10.1109/JMEMS.2017.2712101

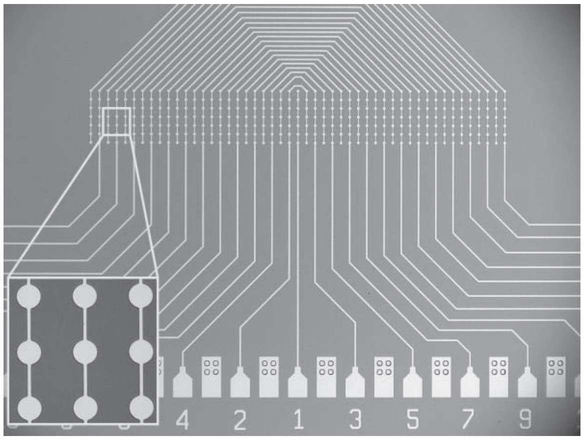

Fig. 2. An optical microscope image of a 7 × 49 PMUT array. The individual PMUTs are 50 μm diameter and the array pitch is 70 μm.

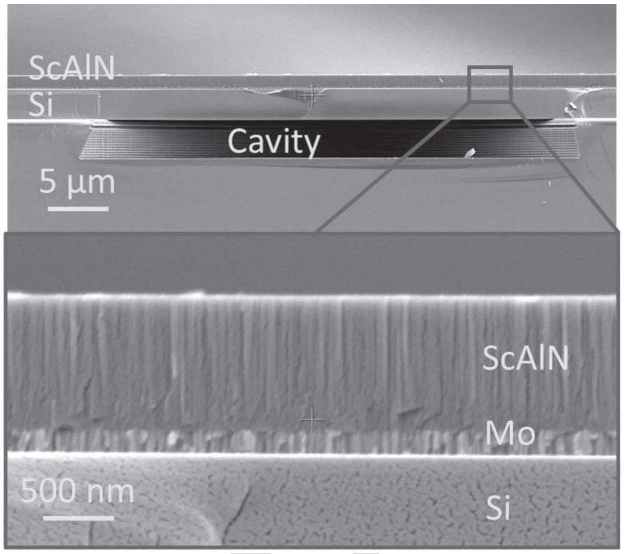

Fig. 3. Cross-sectional SEM image of a ScAlN PMUT. The Mo and ScAlN show good columnar structure indicating a highly c-axis oriented film.

piezoelectric layer, a 200 nm Mo layer as bottom electrode and a 2.5 μm thick silicon membrane. Devices were also fabricated using pure AlN with identical film thicknesses and geometries in order to provide a comparison between ScAlN and AlN PMUTs. The fabrication process used custom cavity SOI (CSOI) substrates wherein vacuum cavities are formed beneath the Si device layer of the CSOI wafer [10]. This process avoids the need for through-wafer etching or sacrificial release layers and eliminates the possible squeeze-film damping between the PMUT membrane and the Si substrate. 150 mm diameter CSOI wafers (IceMOS Technologies) were manufactured with 2 μm deep cavities patterned with diameters from 40 μm to 50 μm and both individual PMUTs and 2D arrays of PMUTs were defined on the wafer. A 7 × 49 array composed of PMUTs with 50 μm diameter and 70 μm pitch is shown in Fig. 2.

The Mo and $Sc_xAl_{1-x}N$ (x = 15%) layers were sputtered in an Advanced Modular Systems (AMS) cluster tool with AlN deposition chambers and ion beam trimming module. The system used a standard dual conical magnetron with an AC deposition source operating at 40 kHz and power varying from 3 to 10 kW. The ScAlN deposition process was in deep poison mode using targets composed of Al and Sc pieces. High purity research grade argon and nitrogen process gases were used for the deposition. The base pressure of the process is ∼5 mTorr and the process temperature is ∼400 °C. Compared to Al-Sc alloy target and multiple targets of Al and Sc, multiple piece targets are easy to make and practical for high volume production. Locally adjusted magnetic field for target pieces of both Al and Sc guaranteed a constant thin film composition over the entire target life. Substrate rotation was utilized to compensate for the variation of the sputtering yield for different materials and composition non-uniformity across the substrate.

The CSOI wafers were cleaned by ion milling first in order to achieve a good interface for the following thin film deposition. A 30 nm thick ScAlN film was first deposited on the CSOI as a seed layer in order to achieve a good crystalline structure of the subsequent Mo and ScAlN layers. Then a 200 nm thick molybdenum (Mo) layer was sputtered as the bottom electrode in a different chamber in the system without breaking vacuum. Finally, 1 μm thick ScAlN was sputtered on the Mo layer. A cross-section scanning electron microscope (SEM) image of a PMUT, Fig. 3, shows the dense columnar structure of the ScAlN film and Mo bottom electrode.

TABLE I
RIE PARAMETERS

Parameter	Values
Cl_2 flow rate (sccm)	90
BCl_3 flow rate (sccm)	30
He flow rate (sccm)	100
TCP RF Power (W)	550
RF Bias Power (W)	150

Following deposition of the ScAlN layer, vias were opened to contact the Mo bottom electrode. AlN films are often etched using heated Microposit MF-319, a positive photoresist developer mainly composed of tetramethylammonium hydroxide (TMAH). However, experiments showed that the ScAlN etch rate in MF-319 was ∼50 nm/min at 60 °C to 70 °C, approximately 4 times slower than that of AlN thin films at the same etching temperature. For this reason, reactive ion etching (RIE) in a transformer coupled plasma (TCP) etcher was studied using a combination of Cl_2 and BCl_3 gases with He used as diluent to improve etch uniformity. A 6.5 μm thick g-line photoresist (OCG 825 35S, Fujifilm) was spin coated, patterned, and hard baked for 16 hours to be used as a mask. An etch rate of 160 nm/min was achieved with the recipe shown in the Table I with an etching selectivity of 0.4 to the mask. Following the via etch, a 200 nm thick aluminum (Al) layer was evaporated and patterned by a lift-off process to form the top electrode and contact pads for the top and bottom electrodes.

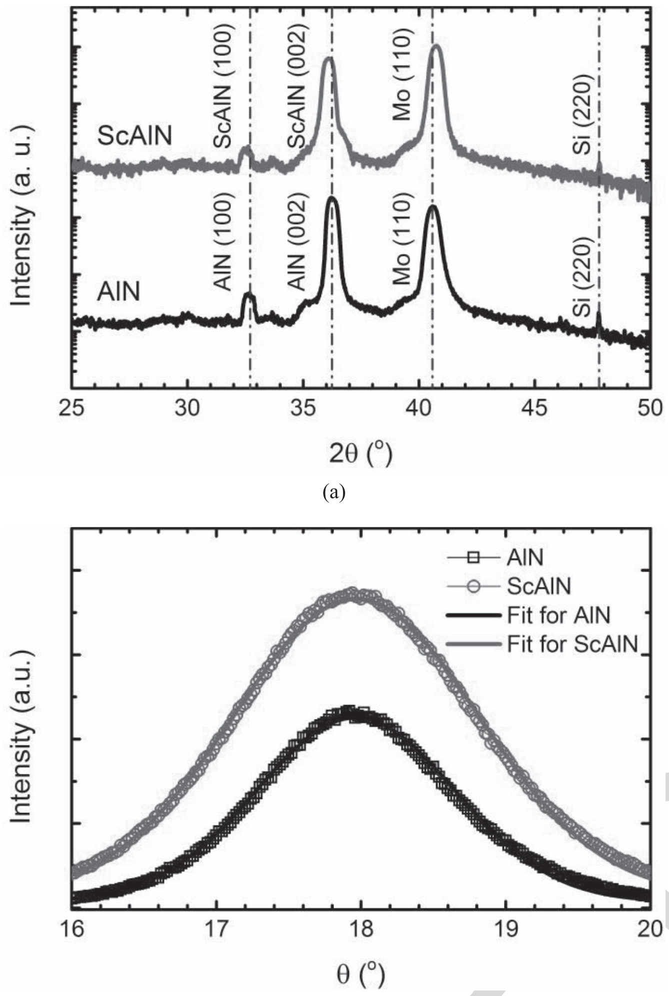

(a)

(b)

Fig. 4. (a) Normal coupled XRD measurement of ScAlN and AlN films in log scale; (b) Rocking curve measurement of the ScAlN and AlN (002) peak in linear scale.

III. RESULTS

A. ScAlN film characterization

The ScAlN crystalline structure was studied using X-ray diffraction (XRD). Fig. 4(a) shows a comparison of the XRD peaks of pure AlN and ScAlN thin films on Mo electrode with 1 μm thickness. The (002) peak and small (100) peak of ScAlN were shifted to a slightly lower angle compared with that of AlN, indicating an expansion of the crystalline lattice according to Bragg's law. The rocking curve of the ScAlN (002) peak was also measured and is shown in Fig. 4(b). The full-width-half-maximum (FWHM) of the (002) peak is 1.6° for the AlN film and 1.9° for the ScAlN film, indicating that the c-axis of the ScAlN film is well aligned and predicting good piezoelectric properties [16].

A focused ion beam (FIB, Scios Dual Beam SEM/FIB system) was utilized to open a trench of approximate dimension 20 μm wide × 20 μm long × 10 μm deep on ScAlN thin film surface. The scandium concentration was measured on the cross section of ScAlN via energy dispersive X-ray spectroscopy (EDX, Oxford Instrument) at 15 keV beam energy. The EDX line-scan data is shown in Fig. 5. The results show a consistent scandium concentration of $x = 15$ at% throughout the thickness of the film. Note that the x-axis position of the EDX intensity in Fig. 5(a) is not exact due to the sample tilt in the SEM.

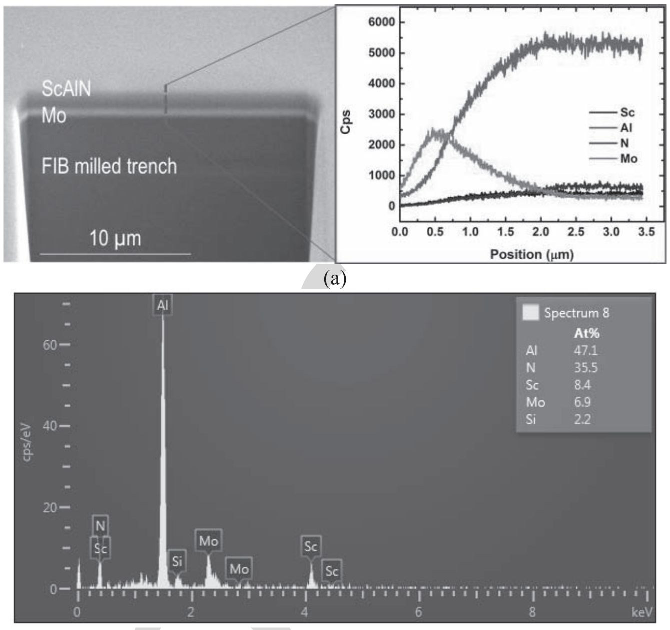

(a)

(b)

Fig. 5. (a) left: SEM image of FIB milled trench on ScAlN surface, right: EDX results over the line scan; (b) EDX results.

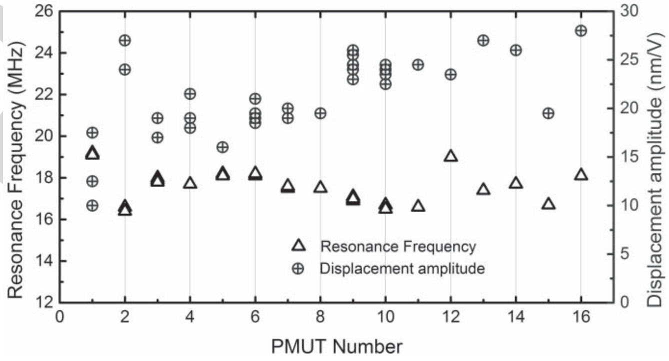

Fig. 6. Measured resonance frequency and dynamic displacement at resonance for ScAlN PMUT with 50 m diameter and 2.5 m nominal Si thickness.

B. Dynamic characterization

The frequency response of ScAlN PMUTs and AlN PMUTs with the same geometry were tested in air using a laser Doppler vibrometer (LDV, OFV 512 and OFV 2700, Polytec) in conjunction with a network analyzer (E5061B, Agilent Technology). LDV measurements were collected on 16 ScAlN PMUTs with 50 μm diameter selected from locations across one wafer, resulting in a 17.5 ± 1.5 MHz natural frequency, 22 ± 4 nm/V peak displacement sensitivity at resonance, and an average quality factor of $Q = 140$ in air. The die to die variation in resonant frequency was within 10% and the variation in amplitude was ∼20%. The results are shown in Fig. 6. Cross-section SEM images showed that

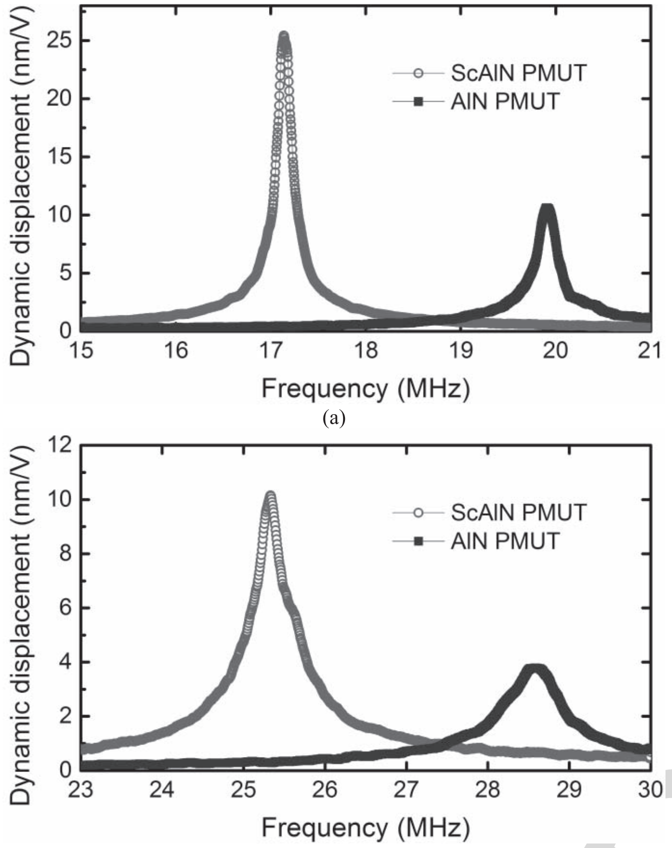

(a)

(b)

Fig. 7. LDV measurement results for (a) 50 μm diameter and (b) 40 μm diameter ScAlN and AlN PMUTs.

the Si thickness of these samples varied from 2.40 μm to 2.93 μm. Fig. 7 compares the LDV results of ScAlN and AlN PMUTs with 50 μm diameter and 40 μm diameter. The peak displacement of the ScAlN PMUTs are more than two times as large as that of the AlN devices.

The difference in the resonance frequency of ScAlN and AlN PMUTs is due to the stiffness reduction from Sc alloying. The resonant frequency of a circular PMUT can be computed from

$$f = \frac{1.63}{r^2}\sqrt{\frac{D}{\sum \rho_i t_i}} \tag{1}$$

where r is the PMUT radius, D is rigidity, ρ and t are the density and thickness of the Si, Mo, and ScAlN layers. The density of $Sc_{0.15}Al_{0.85}N$ is estimated to be 3430 kg/m^3, extrapolated from the density of $Sc_{0.4}Al_{0.6}N$ and AlN [15], [16]. The rigidity D can be expressed as

$$D = \frac{1}{3}\sum_{i=1}^{n} \frac{E_i^2(z_i^3 - z_{i-1}^3)}{1-\upsilon_i^2} \tag{2}$$

where E_i is the Young's modulus and ν_i is the Poisson's ratio of the material, z_i is the distance of the i-th layer top surface from the neutral axis. The Poisson's ratio of $Sc_{0.15}Al_{0.85}N$ in this paper is assumed to be 0.23 [15], [18]. Using (1), the Young's modulus of ScAlN was estimated to be 200 GPa ± 15 GPa, which is consistent with the reported values obtained from ScAlN BAW devices with similar Sc composition [19]. This formula also confirms that the measured variation in natural frequency across the wafer is consistent with the measured variation of the Si device layer thickness.

To extract an estimate of the transverse thin-film piezoelectric coefficient ($e_{31,f}$) from the frequency response data, we normalized the peak displacement by the quality factor, yielding an average value of $d_s = d_p/Q = 180$ pm/V. d_s is related to the transverse piezoelectric coefficient $e_{31,f}$ via [20]:

$$d_s = -r^2\frac{e_{31,f}(t_{si} + t_m + \frac{t_p}{2} - z_n)\cdot I_p(r)}{D\cdot I_d} \tag{3}$$

where t_{si} is the thickness of Si substrate, t_m is the thickness of bottom electrode, t_p is the thickness of ScAlN film, z_n is the distance from the middle of the ScAlN film to neutral axis, and $I_p(r)$ and I_d are integrals related to the piezoelectric bending moment and modal stiffness of the PMUT, both of which depend on the assumed vibration mode shape of the PMUT, $u(r)$,

$$I_p(r_e) = \int_0^{r_e} (r_e\frac{d^2u(r_e)}{dr_e^2} + \frac{du(r_e)}{dr_e})\cdot dr_e \tag{4}$$

$$\begin{aligned} I_d = \int_0^1 [(&\frac{d^2u(r)}{dr^2} + \frac{1}{r}\frac{du(r)}{dr})^2 \\ &-2(1-\upsilon)\frac{1}{r}\frac{du(r)}{dr}\frac{d^2u(r)}{dr^2}]rdr \end{aligned} \tag{5}$$

where υ is Poisson's ratio. $I_p(r_e)$ is a function of r_e, the radius of the circular top electrode normalized to the PMUT radius. Using $u(r) = (1-r^2)^2$ as the assumed mode shape for the 01 vibration mode of a circular membrane, (4) yields $I_p = -1$ at $r_e = 70\%$ and $I_d = 10.67$. Substituting these values along with the geometrical parameters into (3) yields an estimate of $e_{31,f} \sim 1.6$ C/m^2 which is ~60% higher than that of AlN. Our estimated value is consistent with the value extrapolated from [12] measured via a double-side beam interferometry (DBI) and slightly higher than the value extrapolated from [21] measured via a cantilever energy harvester.

Equation (3) also allows the optimum electrode radius for peak displacement to be identified. The estimated material properties including Young's modulus and $e_{31,f}$ were used in (3) to compute the theoretical displacement with r_e varying from 30% to 90%. The results are compared to experimental measurements of PMUTs with varying electrode diameters in Fig. 8, demonstrating good agreement between model and experiment, with the maximum displacement observed with electrode radius from 70% to 80% of the PMUT radius. The difference between theoretical and experimental results at 80% and 90% electrode coverage may be due to inexact boundary conditions (the model assumes perfect clamping at the membrane boundary while some flexing occurs in this location in the real device) or misalignment of the electrode to the silicon membrane (when the electrode covers nearly the whole membrane, an off-center electrode will be partly located on the anchor).

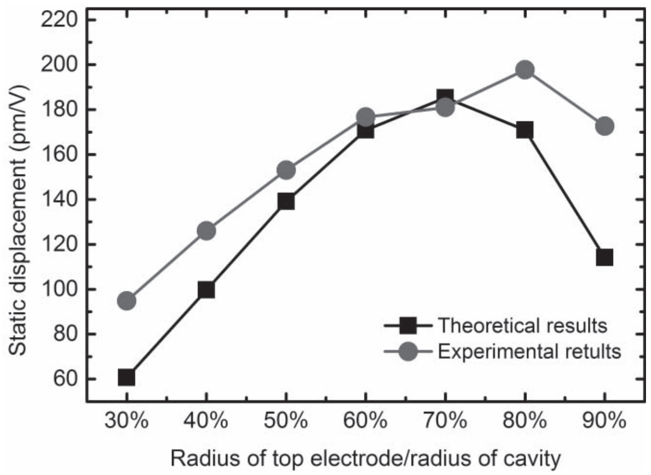

Fig. 8. Theoretical and experimental results of PMUT static displacement with different electrode radius.

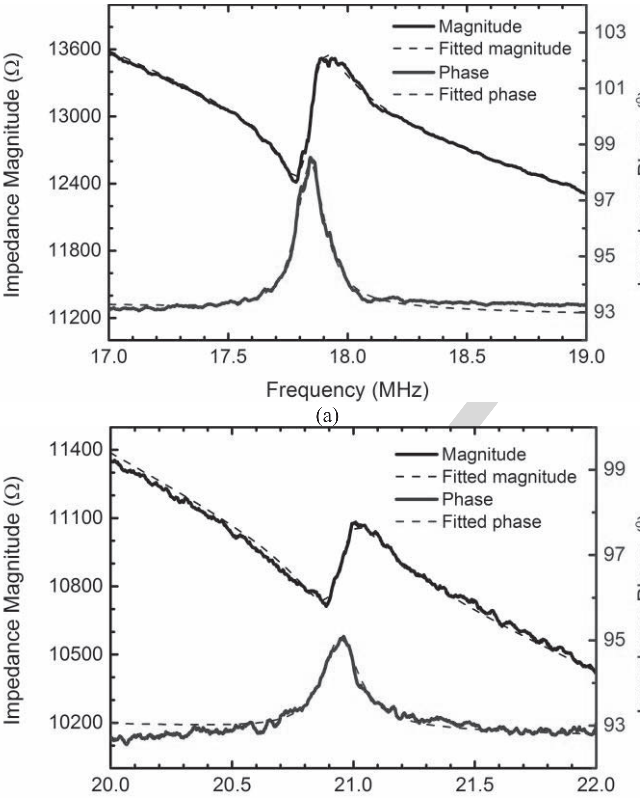

(a)

(b)

Fig. 9. Impedance measurement results for 50 μm diameter (a) ScAlN PMUT and (b) AlN PMUT.

C. Electrical characterization

Impedance measurements of ScAlN and AlN PMUTs, Fig. 9, were performed in air using a GSG RF probe calibrated with an impedance substrate standard (Cascade Microtech). The electromechanical coupling factor k_t^2 was calculated by:

$$k_t^2 = \frac{\pi^2}{4}\frac{f_r}{f_a}\frac{f_a - f_r}{f_a} \tag{6}$$

TABLE II

COMPARISON OF PIEZOELECTRIC MATERIAL PROPERTIES

Materials	$e_{31,f}$ (C/m^2)	ε_{33}	E (GPa)	$\frac{e_{31,f}^2}{\varepsilon_0\varepsilon_{33}}$ (GPa)
PZT [17]	-14.0	1200	65	18.5
AlN (this work)	-1.05	10.5	330	10.8
ScAlN (this work)	-1.6	12	200	24.1

where f_a and f_r are the anti-resonant and resonant frequency respectively. The extracted k_t^2 was 1.9% for ScAlN PMUTs, consistent with the value calculated using the model presented in [20]. For AlN PMUTs, the extracted k_t^2 was 1.4%. This value is higher than the value calculated from the model (modeled AlN $k_t^2 = 0.8\%$). One source of error is that we subtracted the parasitic capacitance of the bond pads and probe setup, and the subtracted parasitic capacitance may have been larger than the true value. Comparing only the two extracted values, we find that the extracted k_t^2 of the ScAlN PMUT is 36% greater than that of AlN. The relative dielectric permittivity (ε_{ScAlN}) of ScAlN was also estimated from the impedance test as ~12 which is around 20% higher than that of pure AlN. The estimated dielectric permittivity is consistent with the value reported in [12].

We also calculated the electromechanical coupling factor using an alternative method to the impedance method described above. The 31 electromechanical coupling coefficient is defined as $k_{31}^2 \propto e_{31,f}^2/\varepsilon_{33}$ [22], [23]. For pulse-echo performance, this metric can be interpreted as follows – the square of the piezocoefficient appears in the numerator because both the TX and RX operations require energy conversion between the electrical and mechanical domains, while the dielectric constant is in the denominator because the RX charge is converted to a voltage by dividing by the capacitance. AlN, ScAlN, and PZT are compared in Table II using the extracted material parameters reported here. Note that while PZT is superior to AlN, the figure-of-merit for ScAlN is 30% greater than that of PZT. One caveat to this conclusion is that the presence of parasitic capacitance (e.g. due to bond-pads or cables between the PMUT and the receive amplifier) will greatly degrade the RX signal amplitude of a ScAlN or AlN PMUT due to the much lower dielectric constant of these materials. For example, a 50 μm diameter PMUT with $r_e = 70\%$ and a 1 μm thick ScAlN layer has a capacitance of 0.1 pF, so the presence of a 1 pF bond-pad capacitance will reduce the RX voltage by a factor of 11 (=0.1 pF /1.1 pF). In comparison, a PZT PMUT of the same size has 100 times greater capacitance, so a 1 pF parasitic capacitance would have negligible effect on the RX voltage.

D. Acoustic characterization

An array of ScAlN PMUTs was immersed in non-conductive fluid (Fluorinert FC-70, 3M) and the output acoustic pressure was measured with a 70 μm diameter needle hydrophone (Precision Acoustic, Inc.). The results are shown

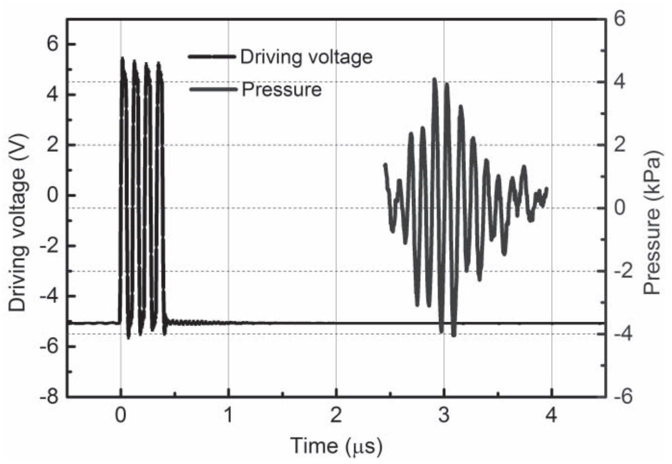

Fig. 10. Pressure measurement results for 7 × 7 ScAlN PMUT array.

TABLE III

COMPARISON OF ACOUSTIC TRANSMISSION PERFORMANCE

Material	Operation Frequency (MHz)	Drive Voltage (V)	Pressure (kPa)	Array size	Normalized output pressure (kPa/V/mm^2)
PZT [10]	10	25	58	9x9	2.52
AlN (this work)	9	25	6	8x8	0.34
ScAlN (this work)	9	11	8	7x7	1.40

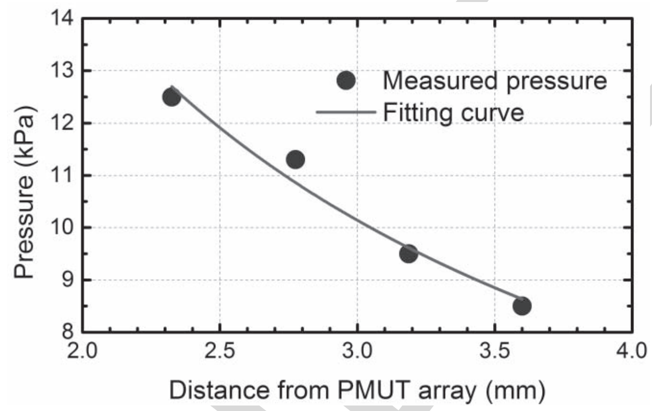

Fig. 11. Acoustic pressure measured from a 15 × 15 PMUT array.

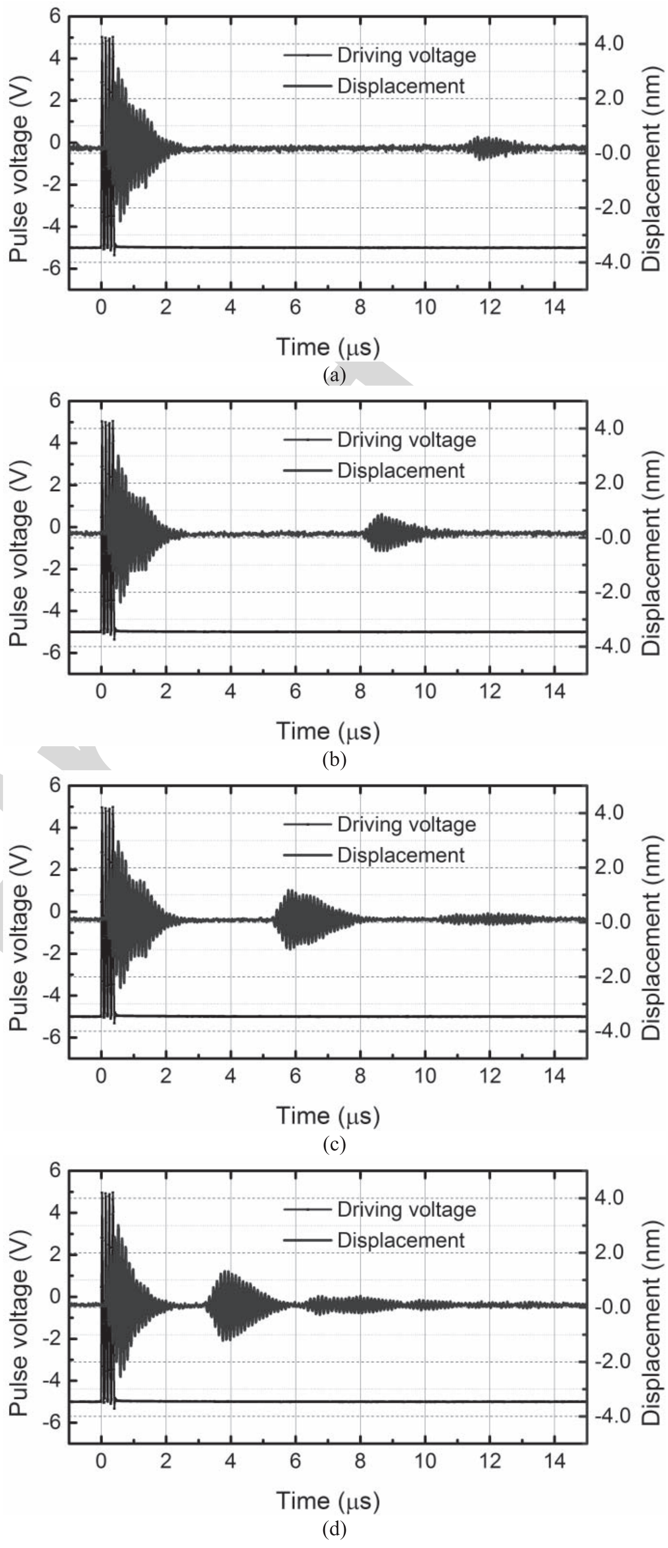

(a)

(b)

(c)

(d)

Fig. 12. LDV measurement of pulse-echo from a ScAlN PMUT in the center of 15 × 15 array with different Fluorinert heights of 4 mm, 3 mm, 2 mm and 1.2 mm.

AQ:2

in Fig. 10. A 7 × 7 ScAlN PMUT array was driven by four 9 MHz 11 Vpp pulses from a function generator (Rigol, DG-4102). The measured pressure generated by the ScAlN PMUT array was detected at ∼2.5 μs after the pulse generation, which corresponds to ∼1.7 mm from the PMUT surface to the hydrophone. The peak-to-peak pressure detected was ∼8 kPa, which was 30% larger than ∼6 kPa pressure generated from a 8 × 8 AlN PMUT array driven at 25 Vpp, suggesting 3x greater transmit efficiency from the ScAlN array. The acoustic transmitting performance of ScAlN, AlN and PZT PMUT arrays were compared as shown in Table III. The normalized output pressure represents the acoustic pressure output from a 1 mm^2 PMUT array area at a distance ∼1.5 mm away from PMUT surface under 1 V driving voltage. The normalized pressure output of the ScAlN PMUT array presented

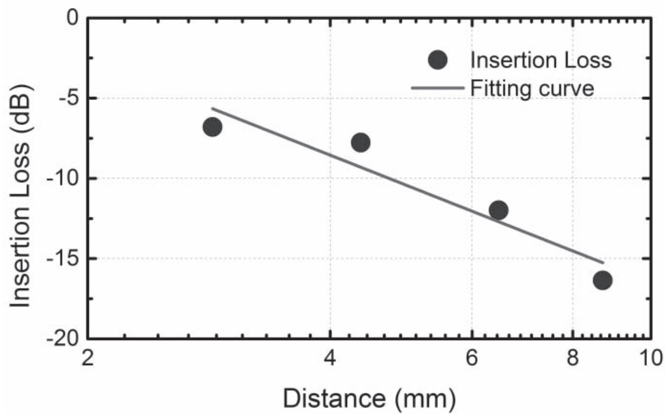

Fig. 13. Measured insertion loss from TX to RX vibration amplitudes as a function of round-trip pulse-echo distance.

here is ∼55% of the PZT array presented in [10]. Considering the much smaller capacitance of ScAlN, we expect that the pulse-echo performance of the PZT and ScAlN arrays should be comparable, because the ScAlN array should have higher receive sensitivity.

The output acoustic pressure of a 15 × 15 ScAlN PMUT array was measured via hydrophone at different distances to PMUT surface. The measured peak-to-peak pressure versus distance is shown in Fig. 11. The result shows that the pressure decays inversely with the radial distance from the array [24]:

$$P\,(r) = P_0 R_0 x^{-1} \tag{7}$$

where R_0 is the Rayleigh distance and P_0 is the theoretical surface pressure. A fit of (7) to the experimental data gives $R_0 = 2.9$ mm and $P_0 = 20.6$ kPa. Given that the peak-to-peak displacement is 5 nm, the value of P_0 gives a transmit sensitivity of $S_{\mathrm{TX}} = 4$ kPa/nm.

The dynamic displacement of a 15 × 15 ScAlN PMUT array driven with 11 Vpp and immersed in fluid was measured via LDV, Fig. 12. An ∼5 nm displacement of the center ScAlN PMUT was measured during the transmit (TX) excitation. PMUT vibration due to received (RX) echoes returning from the fluid-air surface were also visible in these experiments. The Fluorinert-air surface was varied from 4 mm to 1.2 mm, and the plots in Fig. 12 show the echoes return 11 μs, 8 μs, 5 μs and 3 μs after the TX pulse is sent. The corresponding round-trip distances calculated from these pulse echo measurements are consistent with the Fluorinert height using $c = 750$ m/s as the speed of sound in Fluorinert. In Fig. 12(c) and (d), a second echo can be observed due to the short liquid distance and large output pressure. The vibration amplitude of the first received echo relative to the transmit vibration amplitude fits the acoustic spreading model from (7),

$$d_{RX}(x)/d_{TX} = R_0 x^{-1} \tag{8}$$

This model is plotted along with the experimental data in dB units in Fig. 13. Comparing the experimental pressure measurements from Fig. 11 with the RX vibration amplitudes shown in Fig. 12, the receive sensitivity of the array is estimated to be $S_{\mathrm{RX}} = 0.25$ nm/kPa. Since the PMUT is a reciprocal transducer, $S_{\mathrm{TX}} = S_{\mathrm{RX}}^{-1}$, as expected.

IV. CONCLUSION

The results presented here demonstrate that ScAlN PMUTs have better performance than PMUTs made with AlN. Using 15% Sc, the transmit amplitude was increased by a factor of two relative to PMUTs made with pure AlN, consistent with a 60% increase in the transverse piezoelectric coefficient, $e_{31,f}$. The PMUT fabrication process is nearly unchanged by introducing ScAlN. While wet etching of $\mathrm{Sc_{0.15}Al_{0.85}N}$ in TMAH proceeds at a much slower etch rate than pure AlN, a $\mathrm{Cl_2/BCl_3}$plasma etch was demonstrated to achieve an etch rate of 120 nm/min for $\mathrm{Sc_{0.15}Al_{0.85}N}$. We expect that increasing the Sc concentration would further improve PMUT performance, since other work has shown that the piezoelectric coefficients of ScAlN increase as the Sc concentration is increased up to 40%. While RF devices, such as BAW filters, may suffer due to the reduced stiffness (and therefore lower acoustic velocity) that occurs as the Sc concentration is increased, this reduced stiffness does not degrade the performance of PMUTs.

ACKNOWLEDGMENT

The authors thank UC Berkeley Marvel Nanolab for the advice and help on the fabrication process, and IceMOS Technology for providing cavity SOI wafers.

REFERENCES

[1] Q. Wang *et al.*, "Scandium doped aluminum nitride based piezoelectric micromachined ultrasound transducers," in *Proc. Solid-State Sens., Actuators, Microsyst. Workshop*, Hilton Head, SC, USA, 2016, pp. 436–439.

[2] D. E. Dausch, K. H. Gilchrist, J. B. Carlson, S. D. Hall, J. B. Castellucci, and O. T. V. Ramm, "*In vivo* real-time 3-D intracardiac echo using PMUT arrays," *IEEE Trans. Ultrason., Ferroelectr., Freq. Control*, vol. 61, no. 10, pp. 1754–1764, Oct. 2014.

[3] Y. Lu *et al.*, "Waveguide piezoelectric micromachined ultrasonic transducer array for short-range pulse-echo imaging," *Appl. Phys. Lett.*, vol. 106, no. 19, p. 193506, May 2015.

[4] R. J. Przybyla, H. Y. Tang, S. E. Shelton, D. A. Horsley, and B. E. Boser, "3D ultrasonic gesture recognition," in *IEEE Int. Solid-State Circuits Conf. (ISSCC) Dig. Tech. Papers*, Feb. 2014, pp. 210–211.

[5] Y. Lu *et al.*, "Ultrasonic fingerprint sensor using a piezoelectric micromachined ultrasonic transducer array integrated with complementary metal oxide semiconductor electronics," *Appl. Phys. Lett.*, vol. 106, no. 26, p. 263503, 2015.

[6] H.-Y. Tang, Y. Lu, S. Fung, D. A. Horsley, and B. E. Boser, "Integrated ultrasonic system for measuring body-fat composition," in *IEEE Int. Solid-State Circuits Conf. (ISSCC) Dig. Tech. Papers.*, Feb. 2015, pp. 1–3.

[7] D. A. Horsley *et al.*, "Piezoelectric micromachined ultrasonic transducers in consumer electronics: The next little thing?" in *Proc. IEEE 29th Int. Conf. Micro Electro Mech. Syst. (MEMS)*, Jan. 2016, pp. 145–148.

[8] R. Ruby and P. Merchant, "Micromachined thin film bulk acoustic resonators," in *Proc. 48th. IEEE Int. Freq. Control Symp.*, Jun. 1994, pp. 135–138.

[9] J. Zou, C.-M. Lin, Y.-Y. Chen, and A. P. Pisano, "Theoretical study of thermally stable $\mathrm{SiO_2/AlN/SiO_2}$ Lamb wave resonators at high temperatures," *J. Appl. Phys.*, vol. 115, no. 9, p. 094510, Mar. 2014.

[10] Y. Lu and D. A. Horsley, "Modeling, fabrication, and characterization of piezoelectric micromachined ultrasonic transducer arrays based on cavity SOI wafers," *J. Microelectromech. Syst.*, vol. 24, no. 4, pp. 1142–1149, 2015.

[11] Q. Wang, H. Oguchi, M. Hara, and H. Kuwano, "Investigation of dominant factors to control c-axis tilt angle of aln thin films for efficient energy harvesting," in *Proc. IEEE 27th Int. Conf. Micro Electro Mech. Syst. (MEMS)*, Jan. 2014, pp. 636–639.

[12] R. Matloub *et al.*, “Piezoelectric $\mathrm{Al}_{1-x}\mathrm{Sc}_x\mathrm{N}$ thin films: A semiconductor compatible solution for mechanical energy harvesting and sensors,” *Appl. Phys. Lett.*, vol. 102, no. 15, p. 152903, Apr. 2013.

[13] M. Moreira, J. Bjurström, I. Katardjev, and V. Yantchev, “Aluminum scandium nitride thin-film bulk acoustic resonators for wide band applications,” *Vacuum*, vol. 86, no. 1, pp. 23–26, Jul. 2011.

[14] K. Hashimoto, S. Sato, A. Teshigahara, T. Nakamura, and K. Kano, “High-performance surface acoustic wave resonators in the 1 to 3 GHz range using a ScAlN/6H-SiC structure,” *IEEE Trans. Ultrason., Ferroelectr., Freq. Control*, vol. 60, no. 3, pp. 637–642, Mar. 2013, doi: 10.1109/TUFFC.2013.2606

[15] A. Konno *et al.*, “Determination of full material constants of ScAlN thin film from bulk and leaky Lamb waves in MEMS-based samples,” in *Proc. IEEE Int. Ultrason. Symp.*, Sep. 2014, pp. 273–276.

[16] H. P. Loebl, M. Klee, C. Metzmacher, W. Brand, R. Milsom, and P. Lok, “Piezoelectric thin AlN films for bulk acoustic wave (BAW) resonators,” *Mater. Chem. Phys.*, vol. 79, nos. 2–3, pp. 143–146, Apr. 2003.

[17] J.-M. Wagner and F. Bechstedt, “Properties of strained wurtzite GaN and AlN: Ab initio studies,” *Phys. Rev. B, Condens. Matter*, vol. 66, no. 11, p. 115202, Sep. 2002.

[18] A. V. Sotnikov, H. Schmidt, M. Weihnacht, E. P. Smirnova, T. Y. Chemekova, and Y. N. Makarov, “Elastic and piezoelectric properties of AlN and $\mathrm{LiAlO_2}$ single crystals,” *IEEE Trans. Ultrason. Ferroelectr. Freq. Control*, vol. 57, no. 4, pp. 808–811, Apr. 2010.

[19] K. Umeda, H. Kawai, A. Honda, M. Akiyama, T. Kato, and T. Fukura, “Piezoelectric properties of ScAlN thin films for piezo-MEMS devices,” in *Proc. IEEE 26th Int. Conf. Micro Electro Mech. Syst. (MEMS)*, Jan. 2013, pp. 733–736.

[20] M. Dubois and P. Muralt, “PZT thin film actuated elastic fin micromotor,” *IEEE Trans. Ultrason., Ferroelectr., Freq. Control*, vol. 45, no. 5, pp. 1169–1177, Sep. 1998.

[21] P. M. Mayrhofer *et al.*, “ScAlN MEMS cantilevers for vibrational energy harvesting purposes,” *J. Microelectromech. Syst.*, vol. 26, no. 1, pp. 102–112, 2016.

[22] P. Muralt and J. Baborowski, “Micromachined ultrasonic transducers and acoustic sensors based on piezoelectric thin films,” *J. Electroceram.*, vol. 12, nos. 1–2, pp. 101–108, 2004.

[23] K. Smyth and S.-G. Kim, “Experiment and simulation validated analytical equivalent circuit model for piezoelectric micromachined ultrasonic transducers,” *IEEE Trans. Ultrason. Ferroelectr. Freq. Control*, vol. 62, no. 4, pp. 744–765, Apr. 2015.

[24] D. T. Blackstock, *Fundamentals of Physical Acoustics*. Hoboken, NJ, USA: Wiley, 2000.

Qi Wang (S’15) received the B.S. degree in mechanical engineering and automation from the Nanjing University of Aeronautics and Astronautics, Nanjing, China, in 2011, and the M.S. degree in nanomechanics from Tohoku University, Sendai, Japan, in 2013.

He is currently pursuing the Ph.D. degree in mechanical engineering with the Department of Mechanical and Aerospace Engineering, University of California at Davis (UCD), Davis. He is also a Graduate Student Researcher with the Berkeley Sensor and Actuator Center, UCD. His research interests include piezoelectric thin films and MEMS sensors and actuators.

Yipeng Lu received the B.S. degree in materials science and engineering from Jilin University, Changchun, China, in 2007; the M.S. degree in microelectronics from Shanghai Jiao Tong University, Shanghai, China, in 2010, and the Ph.D. degree in mechanical engineering from the University of California at Davis (UCD), Davis, CA, USA, in 2015. He joined the Berkeley Sensor and Actuator Center, UCD, as a Graduate Student Researcher. He was a Digital Hardware Engineer at Huawei in 2011. He is currently a Senior Engineer with Qualcomm. His research interests include MEMS sensors and actuators.

Sergey Mishin received the M.Phys. degree (Hons.) from the Russian National Research University of Electronic Technology in 1986.

His main research interests include cold discharge, high density plasma, magnetron plasma, excimer laser systems, and the application of plasma discharge and lasers in the semi-conductor industry.

He founded Advanced Modular Systems, Inc. in 2000. Advanced Modular Systems, Inc. is responsible for developing the first production worthy cluster tool for high volume piezoelectric thin films. By its second year, Advanced Modular Systems, Inc. was presented with the Supplier of the Year Award by Agilent Technologies, Inc. Since founding his company, he has been focused on the development of new equipment for the manufacture and treatment of piezoelectric thin films. As part of this research and development, he has had an opportunity to work closely with industry leaders and high-class research laboratories. He has also authored or co-authored numerous papers, and holds patents on the deposition and trimming technologies used in FBAR/BAW/SAW and MEMS application.

Yury Oshmyansky received the B.S. and M.S. degrees from the Colorado School of Mines. He was at Hewlett-Packard and subsequently Vitesse, Motorola, SFI, Agilent, Avago, and Advanced Modular Systems, Inc. He is currently the Director of process development with Advanced Modular Systems, Inc. He is also a Chemical Engineer. He holds many patents, and has published numerous papers in the field of manufacturing of the FBAR filters and related technologies. AQ:3

David A. Horsley (M’97) received the B.S., M.S., and Ph.D. degrees in mechanical engineering from the University of California at Berkeley, Berkeley, CA, in 1992, 1994, and 1998, respectively. He has been a Co-Director of the Berkeley Sensor and Actuator Center since 2005. He held research and development positions at Dicon Fiberoptics, Hewlett Packard Laboratories, and Onix Microsystems. He is currently a Professor with the Department of Mechanical and Aerospace Engineering, University of California at Davis, Davis, CA. His research interests include microfabricated sensors and actuators with applications in ultrasonics and physical sensors. He was a recipient of the NSF CAREER Award and the UC Davis College of Engineering’s Outstanding Junior Faculty Award.

AUTHOR QUERIES

AUTHOR PLEASE ANSWER ALL QUERIES

PLEASE NOTE: We cannot accept new source files as corrections for your paper. If possible, please annotate the PDF proof we have sent you with your corrections and upload it via the Author Gateway. Alternatively, you may send us your corrections in list format. You may also upload revised graphics via the Author Gateway.

AQ:1 = Please provide the postal code for "Advanced Modular Systems, Inc."
AQ:2 = Please provide descriptions of all labeled subparts for Fig. 12.
AQ:3 = The term "AMSystems" has been changed to "Advanced Modular Systems, Inc." Please confirm.